PNAS RESEARCH ARTICLE | CHEMISTRY OPEN ACCESS

Many-body effects in the X-ray absorption spectra of liquid water

Fujie Tang[a], Zhenglu Li[b,c], Chunyi Zhang[a], Steven G. Louie[b,c,1], Roberto Car[d,1], Diana Y. Qiu[e,1], and Xifan Wu[a,1]

Contributed by Roberto Car; received January 23, 2022; accepted April 18, 2022; reviewed by Giulia Galli and John Tse

X-ray absorption spectroscopy (XAS) is a powerful experimental technique to probe the local order in materials with core electron excitations. Experimental interpretation requires supporting theoretical calculations. For water, these calculations are very demanding and, to date, could only be done with major approximations that limited the accuracy of the calculated spectra. This prompted an intense debate on whether a substantial revision of the standard picture of tetrahedrally bonded water was necessary to improve the agreement of theory and experiment. Here, we report a first-principles calculation of the XAS of water that avoids the approximations of prior work, thanks to recent advances in electron excitation theory. The calculated XAS spectra, and their variation with changes of temperature and/or with isotope substitution, are in good quantitative agreement with experiments. The approach requires accurate quasiparticle wave functions beyond density functional theory approximations, accounts for the dynamics of quasiparticles, and includes dynamic screening as well as renormalization effects due to the continuum of valence-level excitations. The three features observed in the experimental spectra are unambiguously attributed to excitonic effects. The preedge feature is associated with a bound intramolecular exciton, the main-edge feature is associated with an exciton localized within the coordination shell of the excited molecule, and the postedge feature is delocalized over more distant neighbors, as expected for a resonant state. The three features probe the local order at short, intermediate, and longer range relative to the excited molecule. The calculated spectra are fully consistent with a standard tetrahedral picture of water.

liquid water | X-ray spectroscopy | many-body Green's functions | molecular simulation

Significance

In X-ray absorption spectroscopy, an electron–hole excitation probes the local atomic environment. The interpretation of the spectra requires challenging theoretical calculations, particularly in a system like liquid water, where quantum many-body effects and molecular disorder play an important role. Recent advances in theory and simulation make possible new calculations that are in good agreement with experiment, without recourse to commonly adopted approximations. Based on these calculations, the three features observed in the experimental spectra are unambiguously attributed to excitonic effects with different characteristic correlation lengths, which are distinctively affected by perturbations of the underlying H-bond structure induced by temperature changes and/or by isotopic substitution. The emerging picture of the water structure is fully consistent with the conventional tetrahedral model.

Water is the most important material on Earth. Its structure is defined by a hydrogen bond (H-bond) network whose organization gives rise to its characteristic properties, such as an increased density upon melting, decreased viscosity under pressure, a density maximum at 4 °C, high surface tension, and many more (1, 2). Over decades, numerous advanced experimental techniques have been applied to water in order to reveal the precise character and arrangement of the H-bond network (3–10). Among them, the core-level X-ray absorption spectroscopy (XAS) has emerged as a powerful local probe of the water structure (4, 6, 10–13), which is complementary to the averaged structural information obtained in other scattering experiments. First-principles calculations are indispensable for an unambiguous interpretation of the underlying water structure from the measured spectra (14–24). However, theoretical modeling of XAS in water has proved a challenging subject for the past 20 y. Despite extensive studies, a consensus has yet to be reached (9, 20, 23, 24).

In XAS experiment, a negatively charged core electron is excited by absorbing a high-energy photon, and leaves behind a positively charged core hole with which it can interact to form an exciton (25, 26). The electron–hole interaction is expected to be relatively strong in water, which has a small dielectric constant at characteristic electronic frequencies due to its large band-gap, and the attraction is further strengthened by the disordered liquid structure, which facilitates the localization of the excited electron near the core hole. Consequently, excitonic effects are believed to play an important role in the XAS of water (18, 27–33). In first-principles calculations, the accurate treatment of many-electron effects in two-particle excitations is computationally formidable (34). Most studies, to date, adopt the static core-hole approximation (14–17, 19, 21, 22, 35), which makes the assumption that the hole is described by the static potential of a single core-level atomic orbital, thus simplifying the correlated electron–hole excitation to an equivalent one-particle excitation process. Following this assumption, improved descriptions of the excited electron have been developed and applied in the past decade, where the electron has been treated within an independent electron approximation (16), Slater's transition-state method (14, 15, 36, 37), and self-energy approaches (17, 19, 21, 22, 35). Nevertheless, the reported spectra fluctuate among the

Author contributions: F.T., R.C., D.Y.Q., and X.W. designed research; F.T. performed research; Z.L. and C.Z. contributed new reagents/analytic tools; D.Y.Q. and X.W. analyzed data; and F.T., Z.L., C.Z., S.G.L., R.C., D.Y.Q., and X.W. wrote the paper.

Reviewers: G.G., The University of Chicago; and J.T., University of Saskatchewan.

The authors declare no competing interest.

[1]To whom correspondence may be addressed. Email: sglouie@berkeley.edu, rcar@princeton.edu, diana.qiu@yale.edu, or xifanwu@temple.edu.

This article contains supporting information online at http://www.pnas.org/lookup/suppl/doi:10.1073/pnas.2201258119/-/DCSupplemental.

Published May 13, 2022.

various methods, and discrepancies remain between theory and experiment, raising concerns about the neglect of the core-hole dynamics and resultant renormalization of the core wave function in the presence of electron–hole interactions. This effect can be rigorously accounted for within the GW plus Bethe–Salpeter equation (GW-BSE) method in many-body perturbation theory in which the excitations are correctly described as coherent superpositions of band electron–core hole pairs (27–29, 33, 34, 38, 39). Because of the computational complexity, the full GW-BSE approach has rarely been applied to study the XAS of water. A first attempt was made by Vinson et al. (18) a few years ago, which showed reasonable agreement with experiment. However, the reported spectrum (18) lacks a discernible postedge feature and has a narrower spectral width than experiment.

The current difficulty in reconciling theoretical and experimental spectra reflects long-standing challenges in the theoretical modeling of water, for both the electronic ground state and the excited states. For the ground state, density functional theory (DFT) tends to overestimate the H-bonding strength (40–42). The H bonds form due to a combination of electrostatic attraction and covalency, which originates from the charge transfer between a H-bond donor and acceptor. This charge transfer is greatly overestimated in the generalized gradient approximation of Perdew, Burke, and Ernzerhof (GGA-PBE) DFT functional (43), due to the spurious self-interaction and missing derivative discontinuity of commonly used exchange-correlation (XC) potentials (44, 45). This error is carried over into the calculation of the excited states in conventional GW-BSE calculations, which approximate the quasiparticle (QP) wave functions as the DFT orbitals (34, 38, 39). One way to resolve this is to self-consistently determine the Green's function in the GW approach to obtain the QP wave functions (46–48). Additionally, XAS processes in water are dominated by transitions from the oxygen core-hole state to conduction band states near the Fermi level. At the same photon energies, electrons may also be excited from valence states to high-energy continuum states. Both processes (which couple quantum mechanically to determine the excitation spectrum) are included in experiments (25). However, all theoretical studies thus far have neglected the second process involving the valence to continuum transitions (14–24). A complete treatment of both processes requires one to solve the GW-BSE over the entire Hilbert space of transitions between occupied and unoccupied states consistent with the energy of the photon. In water, this represents a basis of more than 860,000 single-particle states for a box of 32 water molecules. Due to the computational burden, such an effect has yet to be examined in water.

Here, we develop an efficient GW-BSE workflow that allows us to calculate the XAS of liquid water from ab initio with unprecedented accuracy, by combining state-of-the-art methods for both the ground-state—through the use of path-integral deep potential molecular dynamics (PI-DPMD) (49) for the atomic structure—and excited states—through the use of QP wave functions calculated within the static GW approximation, frequency-dependent and fully nonlocal treatment of the dielectric response, and a Hilbert space downfolding approach newly developed to account for the coupling of the core- and valence-level transitions from the electron–hole kernel of the BSE (50, 51). We find that a combination of all these techniques allows us to reproduce the experimental XAS to a high level of accuracy for both the relative energies of the preedge, main-edge, and postedge features and their spectral line shape, and their physical origins. In particular, we find that the use of self-consistent QP wave functions is especially important, since the wave function renormalization due to the electron self-energy promotes intramolecular excitations over intermolecular excitations by reducing the degree of charge transfer in the H bonds. This, in turn, shifts the oscillator strength from the main-edge to the preedge, improving agreement with experiment. Our calculations accurately predict not only the XAS of water but also the subtle changes to the spectrum under elevated temperature and isotope substitution. Our work solves long-existing challenges in the ab initio prediction of the XAS of water, establishing the essential role of electron–hole and many-electron interactions in the prediction of the spectral features and thus drawing an unambiguous path between the excitation spectrum and the underlying molecular structure. The physical understanding and computational approach developed here will be applied in the future to understand XAS experiments in aqueous solutions, confined water, and water at interfaces.

Theoretical XAS of Water

As shown in Fig. 1*A*, we present our theoretical XAS spectrum of liquid water at room temperature. Good agreement can be seen between theory and experiment in both the spectral width and spectral intensities in Fig. 1*A*. In particular, the experimentally observed preedge, main-edge, and postedge features at ∼535 eV, ∼538 eV, and ∼541 eV, respectively, are all well reproduced by the rigorous treatment of electron–hole dynamics. We note that the absolute energies in our calculated spectra are red shifted by ∼16 eV compared to the experimental spectra

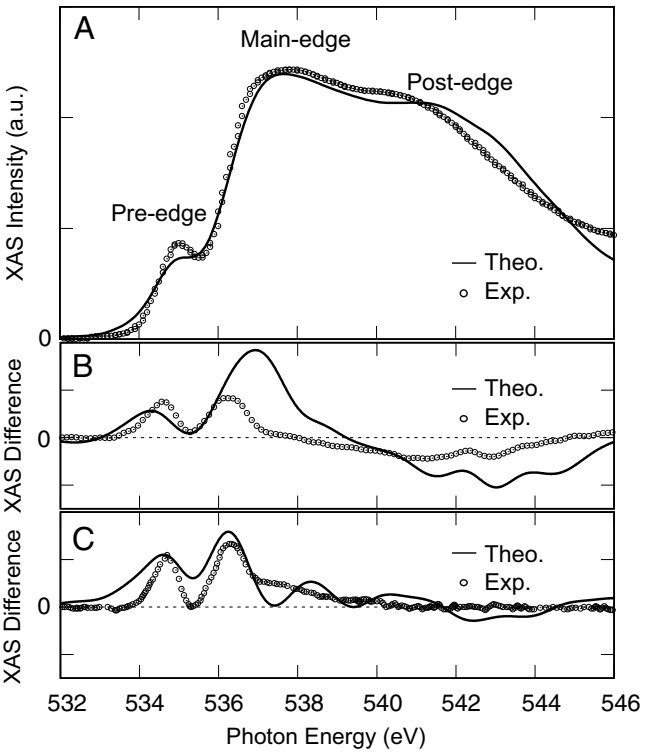

Fig. 1. (*A*) The experimental (Exp., circles) and theoretical (Theo., solid) oxygen K-edge XAS of liquid water. The theoretical XAS was generated at the GW-BSE level using the atomic configuration from a PI-DPMD simulation at 300 K. The experimental data are taken at 296 K from ref. 11. The theoretical spectrum is rigidly shifted by ∼16 eV to align with the preedge peak of the experimental spectrum. The theoretical and experimental spectra are normalized in such a way that they have the same area within the energy range from 532 eV to 546 eV (11, 12). (*B*) Temperature differential spectra: theory (solid line) and experiment (11) (circles). The temperature differences are set to $\Delta T = 30$ K. (*C*) Isotopic differential (H_2O–D_2O) spectra: theory (solid line) and experiment (12) (circles).

(the onset of the theoretical spectrum is 516 eV compared to 532 eV in experiment). This ∼3% discrepancy in the absolute excitation energy is within the expected range of the margin of error of the GW approach for QP energies (52–56). The absolute error of the BSE calculation of exciton binding energies is much smaller, as reflected in the good agreement of the calculated relative peak energies with experiment, since the relevant energy scale is that of the core exciton binding energy on the order of a few electronvolts. To facilitate comparison of features of the calculated and experimental spectra, we aligned all calculated XAS spectra obtained from different individual structures by using the preedge peaks of the corresponding experimental spectra. To analyze the character of the electron–hole excitations, we plot the exciton wave functions for states at various spectral edges (*SI Appendix*, Fig. S8). The electron–hole excitations at the preedge have strong intramolecular character. The excited electron is primarily localized on the same molecule as the core hole (as shown in *SI Appendix*, Fig. S8), so the exciton can be loosely categorized as Frenkel-like. Compared to the preedge, the excited electrons at the main-edge are generally more delocalized. Nevertheless, a certain degree of localization can still be identified. At lower excitation energies near the main-edge, the excited electron is distributed on both the water molecule where the core hole is localized and the H-bonded water molecules in the coordination shell. Therefore, the main-edge is primarily composed of intermolecular electron–hole excitations. In sharp contrast, the electron–hole pairs at postedge are completely delocalized over the cell, which are consistent with resonant exciton states or interband transitions.

Due to the distinct types of excitations associated with each feature, the preedge, main-edge, and postedge of the XAS spectrum convey short-range, intermediate-range, and long-range structural information about the H-bond network of water (9, 10). Thus, XAS can also probe subtle changes in the H-bond network of liquid water due to isotopic and temperature changes. To confirm that our theory captures these changes, we calculate the differential XAS of water under elevated temperature and isotope substitution as presented in Fig. 1 *B* and *C*, respectively. There is good agreement between theory and experiment for both the differential temperature and differential isotopic spectra. As the temperature increases, the coordination of water is further distorted away from an ideal tetrahedron by weakened H bonds, which, in turn, promotes the localization of excitons on the excited water molecule, making both the preedge and main-edge features more prominent. At the same time, the reduced postedge in Fig. 1*B* is consistent with the loss of long-range ordering in the H-bond network at higher temperatures, which is a well-known XAS signature when ice melts into water. On the other hand, the spectral difference between heavy and light water is due to nuclear quantum effects, under which hydrogen explores the configuration space more extensively than the heavier deuterium. As shown in Fig. 1*C*, more pronounced preedge and main-edge features are observed in the differential spectrum between H_2O and D_2O. While the enhancement of these features is similar to the enhancement seen at elevated temperature, the nuclear quantum effects do not have a physical origin identical to the spectral changes, due to elevated temperature. The isotopic changes are due to the higher degree of local disorder of the protons in the light water, both intramolecularly and intermolecularly, which breaks the local tetrahedral coordination and helps localize the electron–hole excitations. The long-range order, as outer shell measured by the oxygen–oxygen distribution functions, is relatively unaffected by this local disorder. Thus, the postedge, which is a signature of long-range ordering, is much less affected by the isotope substitution in Fig. 1*C*. This is consistent with the negligible differences at long-range in the oxygen–oxygen pair distribution functions from neutron scattering experiments (57). The successful reproduction and explanation of these delicate effects suggest our ab initio GW-BSE approach is a reliable theoretical tool to interpret XAS experiments in water.

Many-Body Effects beyond the Conventional GW-BSE Calculation

Importance of Self-Consistent QP in Electron–Hole Interaction. Based on the many-body Green's function method, the GW-BSE approach rigorously treats the electron–hole excitation via an interaction kernel (34, 39) ($K^{eh} = K^d + K^x$, or $K^{eh} = K^d + 2K^x$ for singlet excitations probed by photons in the absence of spin–orbit coupling) composed of both a screened Coulombic attraction K^d and an unscreened exchange repulsion K^x. In conventional calculations (34, 39), the G_0W_0-BSE scheme is often adopted, in which the QP wave functions are approximated by the Kohn–Sham (KS) (58) orbitals that determine the electronic ground state density within DFT. The KS orbitals give only the ground-state density, and not the electronic ground-state wave function, which can be quite different from that of the fictitious KS noninteracting system. In ordinary materials, the G_0W_0-BSE scheme is reasonable as long as the DFT XC functional gives KS orbitals that are close to the QP wave functions (28, 39). However, the above assumption needs to be carefully revisited in water, in view of the sensitivity of the H bonds to the electron delocalization error (44, 45). To some extent, the inclusion of some element of the exact exchange through the use of a hybrid functional may improve the description of the KS orbitals, but it is still expected to suffer from spurious charge delocalization and intrinsic nonlocal and energy-dependent effects of the self-energy operator (49). In principle, the KS orbitals may still be different from the QP wave functions even if one has the exact XC functional and no self-interaction effects.

In water, H bonds are mainly a consequence of the electrostatic attraction between the positive proton and the negative lone electron pair on a neighboring water molecule. The H bond is further stabilized by charge transfer from the occupied orbitals on the H-bond acceptor molecule to virtual orbitals on the H-bond donor molecule. Because the electrostatic contribution to the H bond is rather weak, the charge transfer process contributes considerably to the bonding energy even though it is a higher-order many-body effect (59–61). This charge transfer effect should be well described in an exact DFT. However, the practical implementations of XC potentials partially miss the discrete and quantum nature of electrons, giving rise to the well-known spurious self-interaction and lack of derivative discontinuity in DFT, which results in an overestimation of the charge transfer energy due to overdelocalized and mispositioned electronic states (46–48). Thus, unsurprisingly, in our calculations, the KS DFT orbitals are notably different from the QP wave functions, as evidenced by the large off-diagonal matrix elements of the static Coulomb hole plus screened exchange (COHSEX) self-energy operator in the KS DFT orbital basis, $n|\Sigma(\epsilon^{QP}) - V_{xc}|\bar{n}$ in Fig. 2*B*. The deviations are largest for matrix elements between the occupied p bands and the unoccupied state close to Fermi level, since these are the electronic states involved in the charge transfer processes. The inaccuracy of using the KS DFT orbitals as QP wave functions in the G_0W_0-BSE@PBE calculation is carried over to the electron–hole excitations, resulting in poor agreement with experiment in the XAS

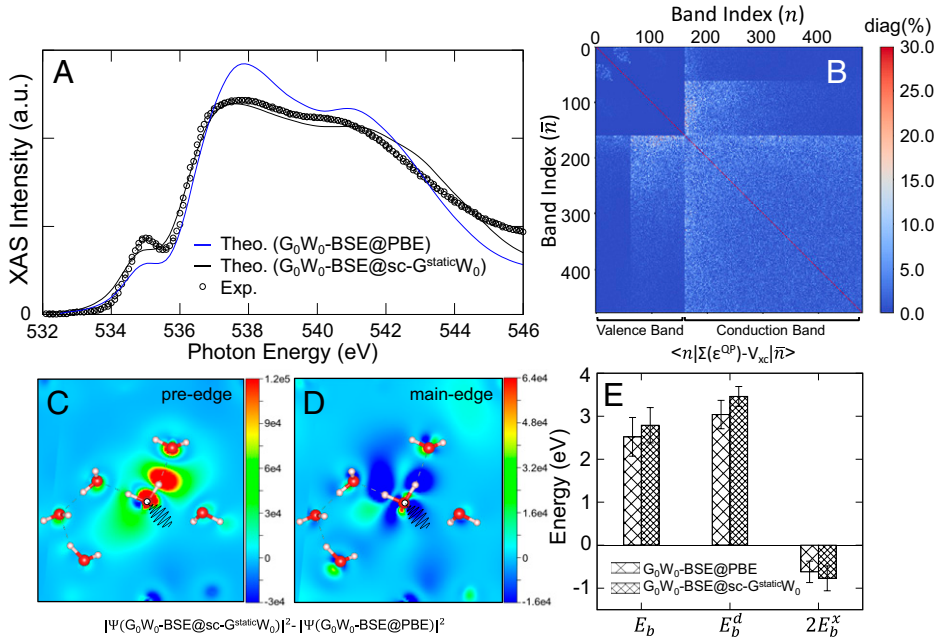

Fig. 2. (*A*) The theoretical XAS of liquid water based on G_0W_0-BSE@PBE (blue) and G_0W_0-BSE@sc-$G^{static}W_0$ (black) approaches. The experimental data (11) are shown with circles. (*B*) Visualization of the matrix elements of the static GW self-energy in the KS DFT basis illustrates the difference between DFT and QP eigenstates. The matrix elements are normalized by the diagonal terms. (*C* and *D*) The two-dimensional contour plot of the electron density ($|\Psi|^2$) difference between G_0W_0-BSE@sc-$G^{static}W_0$ and G_0W_0-BSE@PBE for excitons in the preedge peak (*C*) and main-edge peak (*D*) when the hole is fixed at an oxygen atom (marked with a white circle). The cutting plane is defined as the plane of H_2O with a hole. (*E*) The average exciton binding energy evaluated at the onset of the preedge from the G_0W_0-BSE@PBE and G_0W_0-BSE@sc-$G^{static}W_0$ XAS, together with the contributions of direct term E_b^d and exchange term $2E_b^x$ to the binding energy.

in Fig. 2*A*. The overdelocalized KS DFT orbitals result in an underestimation of the electron–hole interactions at the BSE level. The artificially weakened electron–hole interaction, in turn, gives preferences to intermolecular electron–hole excitons instead of the intramolecular ones. Indeed, compared to experimental data, the XAS spectrum predicted by G_0W_0-BSE@PBE in Fig. 2*A* has a weaker preedge intensity and a more pronounced main-edge intensity. This is consistent with the fact that oscillation strengths are incorrectly transferred from intramolecular to intermolecular excitations.

In order to accurately model the excitonic effect in water, the self-consistent QP wave functions (46–48, 62–66) should be used in describing the electron–hole interaction. Thus, we compute the XAS in water based on the G_0W_0-BSE@sc-$G^{static}W_0$ approach, in which the QP wave functions are obtained by diagonalizing the single-QP Hamiltonian with the static COHSEX self-energy. The adoption of the self-consistent QP wave function reduces the delocalization error of the QP orbitals near the Fermi level, and corrects the overestimated charge transfer process along the H-bond direction in DFT. Consequently, the core hole is more attractive to the excited electrons, thus increasing the oscillator strength of the intramolecular excitons at the preedge. In Fig. 2 *C* and *D*, we present the difference in the electron density of the exciton wave function, when the position of the hole is fixed on a single oxygen atom for exciton states obtained by G_0W_0-BSE@sc-$G^{static}W_0$ and G_0W_0-BSE@PBE approaches, for typical excitations at the preedge and main-edge of the XAS. For the exciton at the preedge in Fig. 2*A*, it can be clearly seen that the excited electron becomes more localized around the excited water molecule, where the hole is positioned. The above largely enhances the intensities of the preedge feature in XAS, resulting in improved agreement with experiment. Consistent with the increased localization near the core hole, the average binding energy at the onset of the preedge evaluated with respect to the QP transition energy is increased by 0.24 eV. Further decomposition of the binding energy (Fig. 2*E*) reveals that the enhanced binding energy ($E_b = E_b^d + 2E_b^x$) is due to the increased direct Coulomb attraction K^d between the oxygen core hole and more localized excited electron state in the self-consistent QP approach. At the same time, the magnitude of the repulsive exchange interaction K^x increases slightly, since the excited electron and hole come closer in real space. As dictated by the optical sum rule, the increased oscillator strength of the preedge feature in G_0W_0-BSE@sc-$G^{static}W_0$ shifts the oscillator strength away from the main-edge and postedge. Therefore, an opposite picture occurs. For a typical electron–hole excitation at the main-edge, the excited electron becomes more delocalized around the excited water molecule in G_0W_0-BSE@sc-$G^{static}W_0$ compared to that predicted by the G_0W_0-BSE@PBE scheme as shown in Fig. 2*D*. The resulting decreased intensities of main-edge and postedge in G_0W_0-BSE@sc-$G^{static}W_0$ again improves agreement between the theoretical XAS and the experimental measurement.

Coupling of Core-Level and Valence-Level Transitions in XAS. Conventional theoretical treatments of XAS only consider a Hilbert space restricted to the occupied states and the lowest unoccupied (conduction) states. We will refer to this as subspace $\mathcal{A}$. Many-body interactions correlate electron–hole excitations in the same energy range (67). Thus, rigorously, the theoretical treatment of core-level spectra within the BSE approach should include not only the core hole and lowest unoccupied states but also their coupling to the manifold of all other transitions with energy in the range of the core-level excitation (subspace $\mathcal{B}$). A proper description of XAS thus demands the modeling of all possible transitions between the initial and final states within the energy of the X-ray photon. As schematically shown in Fig. 3*A*, the complete Hilbert space includes not only transitions between the oxygen 1s core state and the excited electrons in low-energy regions of conduction band as denoted by subspace $\mathcal{A}$ but also

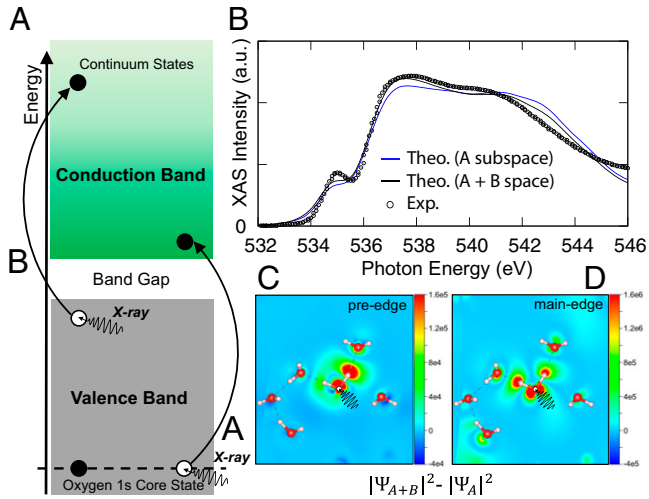

Fig. 3. (*A*) Schematic of the transitions contributing to the experimental XAS measurement: $\mathcal{A}$, between core states and low-lying conduction states; $\mathcal{B}$, between valence states and continuum states. (*B*) The theoretical XAS of liquid water based on the BSE kernel within $\mathcal{A}$ space only (blue) and within $\mathcal{A}\oplus\mathcal{B}$ space (black). The experimental data (11) are shown as circles. (*C* and *D*) The two-dimensional contour plot of the electron density ($|\Psi|^2$) difference of the exciton with the hole fix at an oxygen atom (marked with a white circle) of the preedge (*C*) and main-edge (*D*) peaks between GW-BSE spectra within the $\mathcal{A}$ subspace only and the $\mathcal{A}\oplus\mathcal{B}$ space, respectively. The cutting plane is defined as the plane of H_2O with a hole.

transitions in the subspace $\mathcal{B}$, between the states in the valence band states of water and electrons that are excited to the continuum states in conduction band at much higher energies corresponding to the energy of the X-ray photon (25). The calculation of XAS of water within the entire Hilbert space ($\mathcal{H} = \mathcal{A}\oplus\mathcal{B}$) encounters a significant barrier in computing tens of thousands of QP wave functions, and the subsequent treatment of a large number of electron–hole pair interactions in the BSE is computationally unfeasible within the constraint of current computer resources. Therefore, all theoretical calculations to date (9, 26) have considered only electron–hole pairs within the subspace $\mathcal{A}$, and it was assumed that couplings to the continuum of transitions from subspace $\mathcal{B}$ are small.

Here, we employ a method to account for the coupling between core-level excitons formed within subspace $\mathcal{A}$ and the continuum of valence-level transitions through a matrix downfolding approach. In this approach, the full Hilbert space is downfolded to subspace $\mathcal{A}$. For core excitons, the contribution of the direct Coulomb interaction to the downfolding is small due to the orthogonality of core states in subspace $\mathcal{A}$ and valence states in subspace $\mathcal{B}$. For the exchange interaction, the downfolding is exactly equivalent to screening the exchange term with the polarizability due to electron–hole transitions in subspace $\mathcal{B}$ (50, 51, 68). Using this approach allows us to compute the XAS of liquid water including the coupling of the core–conduction and valence–conduction transitions. Even within this approach, the calculation of the dielectric screening for the downfolding remains a significant computational cost when extended to multiple snapshots of liquid water. Consequently, we perform one fully ab initio calculation of the screened exchange and use that to parametrize a scaling of the exchange interaction that mimics the ab initio screening. (SI Appendix, *Validation of the HL-GPP Model in Liquid Water* for details).

The resulting XAS within the subspace $\mathcal{A}$ only and the downfolded Hilbert space ($\mathcal{H} = \mathcal{A}\oplus\mathcal{B}$) are shown in Fig. 3*B*. It can be clearly seen in Fig. 3*B* that the spectrum generated from the downfolding of the complete Hilbert space is well approximated by the spectrum from subspace $\mathcal{A}$. This is consistent with the expectation that the strong excitonic effects results in a large oscillator strength for the core-level excitons and comparatively weak coupling to the valence continuum. Nevertheless, the transition from subspace $\mathcal{B}$ provides a small but noticeable renormalization effect to the overall XAS. Within the downfolding approach, the renormalization effects from subspace $\mathcal{B}$ are equivalent to applying a screened exchange K^x_{eff} on the coupling of the electron–hole excitations in subspace $\mathcal{A}$. The less repulsive electron–hole interaction means that the overall electron–hole interaction becomes more attractive via the GW-BSE kernel ($K^{\text{eh}} = K^d + K^x_{\text{eff}}$). In particular, the excitons at the preedge and main-edge, respectively, become even more strongly bound around the core hole as shown in Fig. 3 *C* and *D*, which unsurprisingly, yields enhanced oscillator strength at both the preedge and the main edge. With the above renormalization, the intensity at the postedge slightly decreases, as dictated by the optical sum rule. Compared to the conventional XAS computed from subspace $\mathcal{A}$ only, the current theoretical XAS in water considering the full Hilbert space yields a noticeably improved agreement with experiment.

Conclusions

In conclusion, we show that the XAS of liquid water can be accurately predicted by electron–hole excitation theory through the ab initio GW-BSE approach. In addition to the self-energy and excitonic effects, more sophisticated many-body effects beyond conventional one-shot GW-BSE approaches are required for calculations on water, due to the delicate nature of the H-bond network. On the one hand, QP wave functions, obtained by diagonalizing the self-energy operator, should be used instead of the conventional KS DFT orbitals. The employment of self-consistent QP wave functions corrects the overestimated charge transfer processes in DFT and yields significantly improved spectral features. On the other hand, we have also considered electron–hole excitations in the complete Hilbert space, which further yields a noticeable improvement in the agreement of the XAS with experiment. The previously neglected interactions between core-level excitations and the excitations of valence band to a higher-energy conduction band results in a nonnegligible renormalization of the XAS. Interestingly, the agreement of the calculated spectra with experiment showed systematic improvement with the removal of key simplifying approximations.

Our current work provides a rigorous framework for solving the long-standing challenge of modeling the XAS of liquid water from first principles. The accurate predictions from our approach will further help resolve the controversy of the last two decades in the spectral interpretation of the underlying H-bond network. Our simulations show that a fully first-principles approach can lead to XAS spectra in good agreement with experiment without requiring a drastic revision of the standard picture of the tetrahedral H-bond network of water. Furthermore, our work suggests that the high-level many-body effects can play crucial roles in the electron–hole excitations for materials such as water. With further algorithmic optimization and access to advanced computer platforms, the methodologies developed in this work are ready to be widely applied to aqueous systems, such as ionic solutions, confined water, and water at interfaces, as well as other donor–acceptor systems, such as molecular crystals, where the charge transfer effect is important.

Materials and Methods

The molecular structures used in our XAS calculation were extracted from the trajectories of PI-DPMD simulation, where the neural network potential was trained using DFT data based on the hybrid strongly constrained and appropriately normed (SCAN0) XC functional (49). Our PI-DPMD simulations were performed in the canonical ensemble (*NVT*) ensemble at $T = 300$ and 330 K for H_2O and $T = 300$ K for D_2O with periodic boundary conditions. The cubic cell contains 32 water molecules, while the size is adjusted to have the same density as the experimental value. The temperature was controlled by using an eight-bead ring polymer with a color noise path-integral generalized Langevin equation thermostat (i.e., PIGLET) (69) in PI-DPMD. The SCAN0 XC functional is on the fourth rung on Perdew's metaphorical Jacob's ladder (70), which represents the hierarchy of functional approximations in DFT. Previous work showed the predicted water properties are in better agreement with experiment when SCAN0 is used in place of its nonhybrid counterpart (49).

Our GW-BSE XAS calculation was performed using a modified version of the BerkeleyGW (38, 39, 71) package. The multiple-projector norm-conserving pseudopotentials that match the all-electron potentials for oxygen and hydrogen were generated using the Optimized Norm-Conservinng Vanderbilt PSeudopotential (ONCVPSP) package (72). To obtain the QP wave functions, we first calculated the DFT KS orbitals at the level of the GGA-PBE (43) XC functional with a wave function plane wave cutoff of 200 Ry, and then self-consistently updated the wave functions at the GW level in the static limit (static COHSEX). We found that a single self-consistent update was sufficient to obtain the QP wave functions within static COHSEX. Then, a standard one-shot G_0W_0 calculation was performed on top of the static COHSEX QP wave functions and energies. In the G_0W_0 calculation, dielectric screening was included through the full nonlocal dielectric matrix calculated within the random phase approximation. Plane-wave components up to 20 Ry were included in the dielectric matrix, and 10,000 bands were included in the sum over states for the polarizability and the electron self-energy. The frequency dependence in the dielectric matrix was captured using the Hybertsen–Louie generalized plasmon-pole model (38). The BSE calculation based on QP wave function (G_0W_0-BSE@sc-$G^{static}W_0$) for XAS spectra was performed by restricting the BSE basis to transitions between 32 core states (corresponding to the 32 oxygen 1s states) and 160 unoccupied states. Coupling to the space of valence to continuum transitions was included by downfolding the full Hilbert space to the basis on which we solved the BSE (see section, *Coupling of Core-Level and Valence-Level Transition in XAS*). The diagonalization of the BSE Hamiltonian yields the two-particle (electron–hole) exciton states, which were used to construct the XAS, which corresponds to the imaginary part of the dielectric function (ϵ_2). To alleviate the computational burden, we have computed the optical transition matrix elements by using the momentum operator $\boldsymbol{p}$ instead of the velocity operator $\boldsymbol{v}$ in the G_0W_0-BSE@sc-$G^{static}W_0$ approach. The above approximation is equivalent to neglecting the effect of the nonlocality of the pseudopotential (39). In *SI Appendix*, we show that using the matrix elements calculated by the velocity operator $\boldsymbol{v}$ at the level of G_0W_0-BSE@PBE could further improve agreement with experiment. The details of the PI-DPMD simulation and XAS calculations can be found in *SI Appendix*.

Data Availability. All data and codes related to this work, including the DPMD model, molecular snapshots, Quantum Espresso and BerkeleyGW input files, analysis scripts, and instructions to generate figures, are publicly available for download from Figshare (https://figshare.com/articles/dataset/Data_from_Many-Body_Effects_in_the_X-ray_Absorption_Spectra_of_Liquid_Water_/17140172) (73).

ACKNOWLEDGMENTS. This work was primarily supported by the Computational Chemical Center: Chemistry in Solution and at Interfaces funded by the US Department of Energy (DOE) under Award DE-SC0019394, as well as the Computational Materials Science Center: Center for Computational Study of Excited-State Phenomena in Energy Materials funded by the DOE under Contract DE-AC02-05CH11231. The work of F.T., C.Z., R.C., and X.W. on PI-DPMD simulation and XAS calculation was supported by the Computational Chemical Center: Chemistry in Solution and at Interfaces funded by the DOE under Award DE-SC0019394. The work of Z.L., S.G.L., and D.Y.Q. related to implementation of new methodology and algorithms to calculate XAS with the BerkeleyGW code was supported by the Center for Computational Study of Excited-State Phenomena in Energy Materials at the Lawrence Berkeley National Laboratory funded by the DOE under Contract DE-AC02-05CH11231, as part of the Computational Materials Sciences Program. The work of D.Y.Q. on the development of the Hilbert space downfolding approach for core-level spectroscopy was supported by the NSF under Grant DMR-2114081. The work by C.Z. on water structure by neural network potential was supported by the NSF through Award DMR-2053195. This research used resources of the National Energy Research Scientific Computing Center, which is supported by the DOE, Office of Science under Contract DE-AC02-05CH11231. This research used resources of the Oak Ridge Leadership Computing Facility at the Oak Ridge National Laboratory, which is supported by the Office of Science of the DOE under Contract DE-AC05-00OR22725. This research includes calculations carried out on high-performance computing (HPC) resources supported, in part, by the NSF through major research instrumentation Grant 1625061 and by the US Army Research Laboratory under Contract W911NF-16-2-0189.

Author affiliations: [a]Department of Physics, Temple University, Philadelphia, PA 19122; [b]Department of Physics, University of California, Berkeley, CA 94720; [c]Materials Sciences Division, Lawrence Berkeley National Laboratory, Berkeley, CA 94720; [d]Department of Chemistry, Princeton University, Princeton, NJ 08544; and [e]Department of Mechanical Engineering and Materials Science, Yale University, New Haven, CT 06520

1. D. Eisenberg, W. Kauzmann, *The Structure and Properties of Water* (Oxford University Press, New York, 1969).
2. F. H. Stillinger, Water revisited. *Science* **209**, 451–457 (1980).
3. A. K. Soper, M. A. Ricci, Structures of high-density and low-density water. *Phys. Rev. Lett.* **84**, 2881–2884 (2000).
4. P. Wernet *et al.*, The structure of the first coordination shell in liquid water. *Science* **304**, 995–999 (2004).
5. B. Winter *et al.*, Full valence band photoemission from liquid water using EUV synchrotron radiation. *J. Phys. Chem. A* **108**, 2625–2632 (2004).
6. J. S. Tse *et al.*, X-ray Raman spectroscopic study of water in the condensed phases. *Phys. Rev. Lett.* **100**, 095502 (2008).
7. H. J. Bakker, J. L. Skinner, Vibrational spectroscopy as a probe of structure and dynamics in liquid water. *Chem. Rev.* **110**, 1498–1517 (2010).
8. F. Perakis *et al.*, Vibrational spectroscopy and dynamics of water. *Chem. Rev.* **116**, 7590–7607 (2016).
9. T. Fransson *et al.*, X-ray and electron spectroscopy of water. *Chem. Rev.* **116**, 7551–7569 (2016).
10. J. W. Smith, R. J. Saykally, Soft X-ray absorption spectroscopy of liquids and solutions. *Chem. Rev.* **117**, 13909–13934 (2017).
11. J. Meibohm, S. Schreck, P. Wernet, Temperature dependent soft x-ray absorption spectroscopy of liquids. *Rev. Sci. Instrum.* **85**, 103102 (2014).
12. S. Schreck, P. Wernet, Isotope effects in liquid water probed by transmission mode x-ray absorption spectroscopy at the oxygen K-edge. *J. Chem. Phys.* **145**, 104502 (2016).
13. M. R. Carbone, M. Topsakal, D. Lu, S. Yoo, Machine-learning x-ray absorption spectra to quantitative accuracy. *Phys. Rev. Lett.* **124**, 156401 (2020).
14. B. Hetényi, F. De Angelis, P. Giannozzi, R. Car, Calculation of near-edge x-ray-absorption fine structure at finite temperatures: Spectral signatures of hydrogen bond breaking in liquid water. *J. Chem. Phys.* **120**, 8632–8637 (2004).
15. M. Cavalleri, M. Odelius, A. Nilsson, L. G. M. Pettersson, X-ray absorption spectra of water within a plane-wave Car-Parrinello molecular dynamics framework. *J. Chem. Phys.* **121**, 10065–10075 (2004).
16. D. Prendergast, G. Galli, X-ray absorption spectra of water from first principles calculations. *Phys. Rev. Lett.* **96**, 215502 (2006).
17. W. Chen, X. Wu, R. Car, X-ray absorption signatures of the molecular environment in water and ice. *Phys. Rev. Lett.* **105**, 017802 (2010).
18. J. Vinson, J. J. Kas, F. D. Vila, J. J. Rehr, E. L. Shirley, Theoretical optical and x-ray spectra of liquid and solid H_2O. *Phys. Rev. B Condens. Matter Mater. Phys.* **85**, 045101 (2012).
19. L. Kong, X. Wu, R. Car, Roles of quantum nuclei and inhomogeneous screening in the x-ray absorption spectra of water and ice. *Phys. Rev. B Condens. Matter Mater. Phys.* **86**, 134203 (2012).
20. T. Fransson *et al.*, Requirements of first-principles calculations of X-ray absorption spectra of liquid water. *Phys. Chem. Chem. Phys.* **18**, 566–583 (2016).
21. Z. Sun *et al.*, X-ray absorption of liquid water by advanced ab initio methods. *Phys. Rev. B* **96**, 104202 (2017).
22. Z. Sun *et al.*, Electron-hole theory of the effect of quantum nuclei on the x-ray absorption spectra of liquid water. *Phys. Rev. Lett.* **121**, 137401 (2018).
23. I. Zhovtobriukh, N. A. Besley, T. Fransson, A. Nilsson, L. G. M. Pettersson, Relationship between x-ray emission and absorption spectroscopy and the local H-bond environment in water. *J. Chem. Phys.* **148**, 144507 (2018).
24. I. Zhovtobriukh, P. Norman, L. G. M. Pettersson, X-ray absorption spectrum simulations of hexagonal ice. *J. Chem. Phys.* **150**, 034501 (2019).
25. L. G. Parratt, Electronic band structure of solids by x-ray spectroscopy. *Rev. Mod. Phys.* **31**, 616–645 (1959).
26. J. J. Rehr, R. C. Albers, Theoretical approaches to x-ray absorption fine structure. *Rev. Mod. Phys.* **72**, 621–654 (2000).
27. W. Olovsson, I. Tanaka, T. Mizoguchi, P. Puschnig, C. Ambrosch-Draxl, All-electron Bethe-Salpeter calculations for shallow-core x-ray absorption near-edge structures. *Phys. Rev. B* **79**, 041102(R) (2009).

28. J. Vinson, J. J. Rehr, J. J. Kas, E. L. Shirley, Bethe-Salpeter equation calculations of core excitation spectra. *Phys. Rev. B Condens. Matter Mater. Phys.* **83**, 115106 (2011).
29. A. Gulans *et al.*, Exciting: A full-potential all-electron package implementing density-functional theory and many-body perturbation theory. *J. Phys. Condens. Matter* **26**, 363202 (2014).
30. C. Vorwerk, F. Sottile, C. Draxl, Excitation pathways in resonant inelastic x-ray scattering of solids. *Phys. Rev. Res.* **2**, 042003(R) (2020).
31. S. Ono, Y. Noguchi, R. Sahara, Y. Kawazoe, K. Ohno, TOMBO: All-electron mixed-basis approach to condensed matter physics. *Comput. Phys. Commun.* **189**, 20–30 (2015).
32. Y. Noguchi, M. Hiyama, H. Akiyama, Y. Harada, N. Koga, First-principles investigation of strong excitonic effects in oxygen 1s X-ray absorption spectra. *J. Chem. Theory Comput.* **11**, 1668–1673 (2015).
33. C. Vorwerk, C. Cocchi, C. Draxl, Addressing electron-hole correlation in core excitations of solids: An all-electron many-body approach from first principles. *Phys. Rev. B* **95**, 155121 (2017).
34. G. Onida, L. Reining, A. Rubio, Electronic excitations: Density-functional versus many-body Green's-function approaches. *Rev. Mod. Phys.* **74**, 601–659 (2002).
35. C. Zhang *et al.*, Isotope effects in x-ray absorption spectra of liquid water. *Phys. Rev. B* **102**, 115155 (2020).
36. J. C. Slater, J. B. Mann, T. M. Wilson, J. H. Wood, Nonintegral occupation numbers in transition atoms in crystals. *Phys. Rev.* **184**, 672–694 (1969).
37. J. C. Slater, J. H. Wood, Statistical exchange and the total energy of a crystal. *Int. J. Quantum Chem.* **5**, 3–34 (1970).
38. M. S. Hybertsen, S. G. Louie, Electron correlation in semiconductors and insulators: Band gaps and quasiparticle energies. *Phys. Rev. B Condens. Matter* **34**, 5390–5413 (1986).
39. M. Rohlfing, S. G. Louie, Electron-hole excitations and optical spectra from first principles. *Phys. Rev. B Condens. Matter Mater. Phys.* **62**, 4927–4944 (2000).
40. T. D. Kühne, M. Krack, M. Parrinello, Static and dynamical properties of liquid water from first principles by a novel Car-Parrinello-like approach. *J. Chem. Theory Comput.* **5**, 235–241 (2009).
41. R. A. DiStasio Jr., B. Santra, Z. Li, X. Wu, R. Car, The individual and collective effects of exact exchange and dispersion interactions on the ab initio structure of liquid water. *J. Chem. Phys.* **141**, 084502 (2014).
42. M. Chen *et al.*, Ab initio theory and modeling of water. *Proc. Natl. Acad. Sci. U.S.A.* **114**, 10846–10851 (2017).
43. J. P. Perdew, K. Burke, M. Ernzerhof, Generalized gradient approximation made simple. *Phys. Rev. Lett.* **77**, 3865–3868 (1996).
44. A. J. Cohen, P. Mori-Sánchez, W. Yang, Insights into current limitations of density functional theory. *Science* **321**, 792–794 (2008).
45. A. J. Cohen, P. Mori-Sánchez, W. Yang, Challenges for density functional theory. *Chem. Rev.* **112**, 289–320 (2012).
46. F. Caruso *et al.*, First-principles description of charge transfer in donor-acceptor compounds from self-consistent many-body perturbation theory. *Phys. Rev. B Condens. Matter Mater. Phys.* **90**, 085141 (2014).
47. C. Faber, P. Boulanger, I. Duchemin, C. Attaccalite, X. Blase, Many-body Green's function GW and Bethe-Salpeter study of the optical excitations in a paradigmatic model dipeptide. *J. Chem. Phys.* **139**, 194308 (2013).
48. F. Kaplan, F. Weigend, F. Evers, M. J. van Setten, Off-diagonal self-energy terms and partially self-consistency in GW calculations for single molecules: Efficient implementation and quantitative effects on ionization potentials. *J. Chem. Theory Comput.* **11**, 5152–5160 (2015).
49. C. Zhang *et al.*, Modeling liquid water by climbing up Jacob's ladder in density functional theory facilitated by using deep neural network potentials. *J. Phys. Chem. B* **125**, 11444–11456 (2021).
50. L. X. Benedict, Screening in the exchange term of the electron-hole interaction of the Bethe-Salpeter equation. *Phys. Rev. B Condens. Matter Mater. Phys.* **66**, 193105 (2002).
51. D. Y. Qiu, F. H. Da Jornada, S. G. Louie, Solving the Bethe-Salpeter equation on a subspace: Approximations and consequences for low-dimensional materials. *Phys. Rev. B* **103**, 045117 (2021).
52. M. J. van Setten *et al.*, GW100: Benchmarking G0W0 for molecular systems. *J. Chem. Theory Comput.* **11**, 5665–5687 (2015).
53. X. Ren *et al.*, Resolution-of-identity approach to Hartree-Fock, hybrid density functionals, RPA, MP2 and GW with numeric atom-centered orbital basis functions. *New J. Phys.* **14**, 053020 (2012).
54. L. Hedin, On correlation effects in electron spectroscopies and the GW approximation. *J. Phys. Condens. Matter* **11**, R489 (1999).
55. F. Aryasetiawan, O. Gunnarsson, The GW method. *Rep. Prog. Phys.* **61**, 237–312 (1998).
56. F. Viñes, C. Sousa, F. Illas, On the prediction of core level binding energies in molecules, surfaces and solids. *Phys. Chem. Chem. Phys.* **20**, 8403–8410 (2018).
57. A. K. Soper, C. J. Benmore, Quantum differences between heavy and light water. *Phys. Rev. Lett.* **101**, 065502 (2008).
58. W. Kohn, L. J. Sham, Self-consistent equations including exchange and correlation effects. *Phys. Rev.* **140**, A1133–A1138 (1965).
59. R. Z. Khaliullin, A. T. Bell, M. Head-Gordon, Analysis of charge transfer effects in molecular complexes based on absolutely localized molecular orbitals. *J. Chem. Phys.* **128**, 184112 (2008).
60. R. Z. Khaliullin, A. T. Bell, M. Head-Gordon, Electron donation in the water-water hydrogen bond. *Chemistry* **15**, 851–855 (2009).
61. A. J. Misquitta, Charge transfer from regularized symmetry-adapted perturbation theory. *J. Chem. Theory Comput.* **9**, 5313–5326 (2013).
62. F. Bruneval, N. Vast, L. Reining, Effect of self-consistency on quasiparticles in solids. *Phys. Rev. B Condens. Matter Mater. Phys.* **74**, 045102 (2006).
63. M. Gatti, F. Bruneval, V. Olevano, L. Reining, Understanding correlations in vanadium dioxide from first principles. *Phys. Rev. Lett.* **99**, 266402 (2007).
64. J. Vidal, F. Trani, F. Bruneval, M. A. L. Marques, S. Botti, Effects of electronic and lattice polarization on the band structure of delafossite transparent conductive oxides. *Phys. Rev. Lett.* **104**, 136401 (2010).
65. J. Vidal, S. Botti, P. Olsson, J. F. Guillemoles, L. Reining, Strong interplay between structure and electronic properties in CuIn(S,Se)$_2$: A first-principles study. *Phys. Rev. Lett.* **104**, 056401 (2010).
66. T. Rangel *et al.*, Band structure of gold from many-body perturbation theory. *Phys. Rev. B Condens. Matter Mater. Phys.* **86**, 125125 (2012).
67. U. Fano, J. W. Cooper, Spectral distribution of atomic oscillator strengths. *Rev. Mod. Phys.* **40**, 441–507 (1968).
68. T. Deilmann, K. S. Thygesen, Important role of screening the electron-hole exchange interaction for the optical properties of molecules near metal surfaces. *Phys. Rev. B* **99**, 045133 (2019).
69. M. Ceriotti, G. Bussi, M. Parrinello, Nuclear quantum effects in solids using a colored-noise thermostat. *Phys. Rev. Lett.* **103**, 030603 (2009).
70. J. P. Perdew, Jacob's ladder of density functional approximations for the exchange-correlation energy. *AIP Conf. Proc.* **577**, 1–20 (2001).
71. J. Deslippe *et al.*, BerkeleyGW: A massively parallel computer package for the calculation of the quasiparticle and optical properties of materials and nanostructures. *Comput. Phys. Commun.* **183**, 1269–1289 (2012).
72. D. R. Hamann, Optimized norm-conserving Vanderbilt pseudopotentials. *Phys. Rev. B Condens. Matter Mater. Phys.* **88**, 085117 (2013).
73. F. Tang *et al.*, Data from "Many-body effects in the X-ray absorption spectra of liquid water." Figshare. https://figshare.com/articles/dataset/Data_from_Many-Body_Effects_in_the_X-ray_Absorption_Spectra_of_Liquid_Water_/17140172. Deposited 12 December 2021.